Optics Communications 331 (2014) 98–104

Contents lists available at ScienceDirect

Optics Communications

journal homepage: www.elsevier.com/locate/optcom

Role of Er^{3+} ion concentration and incoherent pumping field on optical bistability in Er^{3+}:YAG crystal

Seyyed Hossein Asadpour*, H. Rahimpour Soleimani

Department of Physics, University of Guilan, Rasht, Iran

ARTICLE INFO

Article history:
Received 2 March 2014
Received in revised form
22 May 2014
Accepted 27 May 2014
Available online 11 June 2014

Keywords:
Optical bistability
Er^{3+} concentration
Incoherent pumping

ABSTRACT

In this paper, two atomic models are proposed in an 35 nm Er^{3+}-doped YAG crystal. The effect of Er^{3+} ion concentration and incoherent pumping field on optical bistability is discussed. The results for two models show that the threshold of optical bistability for some Er^{3+} concentration reduces and for some concentration increases. We display that the incoherent pumping field makes the behavior of optical bistability for two proposed model completely different at identical conditions for Er^{3+} concentration. Our results show that in the absence and presence of incoherent pumping field some Er^{3+} concentration can lead to maximum and minimum OB threshold. We hope that our proposed model can be suitable for optimizing and controlling the optical bistability in Er^{3+}:YAG crystal.

1. Introduction

It is known that for the next generation of all-optical systems controlling light by light is important in photonics. In this case, quantum coherence and interference has essential roles. Some interesting phenomena which resulted from quantum coherence and interference have been studied theoretically and experimentally by many research groups. For example, electromagnetically induced transparency (EIT) [1,2], lasing without inversion (LWI) [3], slow and fast light [4], four wave mixing (FWM) [5–7], optical solitons [8,9], optical bistability (OB) [10–15] and many other interesting phenomena [16–25] have been analyzed. Recently, optical bistability has drawn considerable interest due its potential applications in the future photonic devices. Based on atomic coherence and quantum interference, many proposals have been proposed for optical bistability and multistability in atomic systems. Li et al. [10] showed that quantum interference can be used to modify intensity threshold of optical bistability and multistability. Joshi and Xiao showed that OB in multi-level systems has advantages over the two-level systems [11]. Osman and Joshi [14] showed that with incoherent pumping field and spontaneously generated coherence (SGC) the OB was investigated under mean field approximation. In another study by Osman [13], it is shown that the optical multistability can occur in a ring cavity for the V-type atomic system, driven by a coherent field and control field (coherent+dc fields). It is found that in the presence of dc field has a dominant effect on generating the optical multistability of the system. Also it is shown that the effects of the quantum interference from spontaneous emission of the relative phase between the two fields of the control field might be of use to control the threshold value and width of the hysteresis cycle, which can adjust the optical switching process when they are taken at optimal values. In our recent work [15], we discussed the absorption spectrum, transmission coefficient and optical bistability in a four-level inverted Y-type atomic system. Our results showed that the transmission on or off the two orthogonally polarized beams at different frequencies can be achieved by external magnetic field.

Recently, it is shown that similar phenomena involving quantum coherence and quantum interference in solid state systems have also attracted great attention due to the potentially important applications in optoelectronics and solid state information sciences [26,27]. It has been shown that they can lead to EIT [28–30], gain without inversion [31–33], coherently controlled photocurrent generation [34], optical bistability and multistability [35–46,55]. It has been shown that the OB threshold intensity can be significantly controlled by effect of quantum coherence and interference in semiconductor nanostructure. For example, Li studied the behavior of OB in a triple semiconductor quantum well structure with tunneling induced interference [35] and Wang and Yu reported OB behavior in an asymmetric three-coupled quantum well inside a unidirectional ring cavity via coherent driven field [43].

The observation of coherent phenomena such as EIT and LWI in semiconductor materials are difficult due their large ($\sim 100\, fs^{-1}$) dephasing rates. However, devices based on intersubband transitions in semiconductor quantum well structure have many inherent advantages, such as large electric dipole moments due to the

* Corresponding author. Tel./fax: +98 1313220066.
E-mail address: S.Hosein.Asadpour@gmail.com (S.H. Asadpour).

http://dx.doi.org/10.1016/j.optcom.2014.05.059
0030-4018/

small effective electron mass, high nonlinear optical coefficients, and a great flexibility in device design by choosing the materials and structure dimensions. Furthermore, the transition energies, dipoles, and symmetries can be engineered. Note that the implementation of EIT in semiconductor-based devices is very attractive from view point of applications. The theory of quantum coherence phenomena in semiconductor quantum dots (SQDs) was also introduced by Chow and Kim [47,48].

In addition, rare-earth-doped crystals have properties similar to atomic vapors but with the advantage of no atomic diffusion. Yttrium aluminum garnet is an excellent optical host material compared with others. Er^{+3}-doped YAG crystal is an efficient active medium for lasers operating in the middle infrared band, coinciding with the telecommunications band. Furthermore, our study is much more useful than its gaseous equal due to its flexible design and the wide modifiable parameters. Therefore, our schemes are very suitable for experimental understanding. Quantum interference and quantum coherence phenomena such as EIT [49–51], large refractive index without absorption [27], enhanced Kerr nonlinearity [52], lasing with and without population inversion [53], controlling the intensity threshold of optical bistability [54,55] and all-optical switching [56–59] have been also studied in rare-earth-doped crystals. For example as per Ref. [56], Zang proposed all-optical switching based on a Signac loop mirror that incorporates a ytterbium-doped fiber and uniform fiber Bragg grating (FBG). It was found that transmission spectrum of this structure is the narrow splitting of the reflection spectrum of the FBG. The shift of this ultranarrow transmission spectrum is very sensitive to the intensity of the pump power. Thus, the threshold switching power can be greatly reduced by shifting such narrow transmission spectrum. In another paper by Zang et al. [57], an all-optical switching device, which is constructed by connecting an erbium-doped fiber with two symmetrical long-period fiber gratings (EDF–LPFGs), was demonstrated. It was shown that the threshold switching power is inversely proportional to the nonlinear coefficient of the erbium-doped fiber, and is proportional to the effective area of the erbium-doped fiber and absorption coefficient.

In this paper, we propose two four-level atomic configurations in 35 nm Er^{3+}:YAG crystal and analyze the simultaneous effects of incoherent pumping field and Er^{3+} ion concentration on intensity threshold of optical bistability. We show that in the presence and absence of incoherent pumping field and for two different proposed atomic configurations in Er^{3+}:YAG crystal, the Er^{3+} ion concentration has differential effects on optical bistability. To the best of our knowledge, the effect of Er^{3+} ion concentration on OB is not considered by any research group. We hope that our theoretical results are helpful for the future experimental investigations.

2. The model and equations

In this section, we propose two configurations for OB and OM as depicted in Figs. 1 and 2.

2.1. Scheme 1

Consider a four-level Er^{3+} ionic system in an 35 nm Er^{3+}-doped YAG crystal as shown in Fig. 1. The energy-level scheme is relevant to the Er^{3+} ions in Er^{3+}:YAG crystal, where levels $|1\rangle$, $|2\rangle$, $|3\rangle$ and $|4\rangle$ correspond to energy levels of Er^{3+} ions $^4I_{15/2}$, $^4I_{13/2}$, $^4I_{11/2}$, and $^4I_{9/2}$, respectively. Details of the level structure and the corresponding transition wavelength can be found in Ref. [55]. In this scheme, a strong coupling field drives $|2\rangle \leftrightarrow |4\rangle$ transition. A weak probe field couples the $|1\rangle \rightarrow |2\rangle$ transition. An incoherent pumping field with pumping rate r applies between levels $|1\rangle$ and $|3\rangle$. With the usual

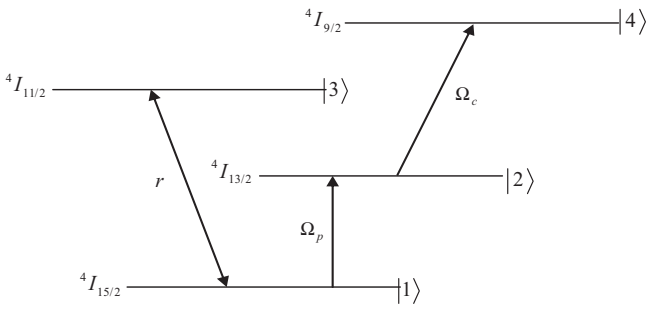

Fig. 1. The Er^{3+}:YAG crystal interacts with two laser fields and an incoherent pump. Probe field couples $|1\rangle \leftrightarrow |2\rangle$ transition, and control field drives $|2\rangle \leftrightarrow |4\rangle$ transition. An incoherent pump field with the pumping rate r is acting on $|1\rangle \leftrightarrow |3\rangle$ transition.

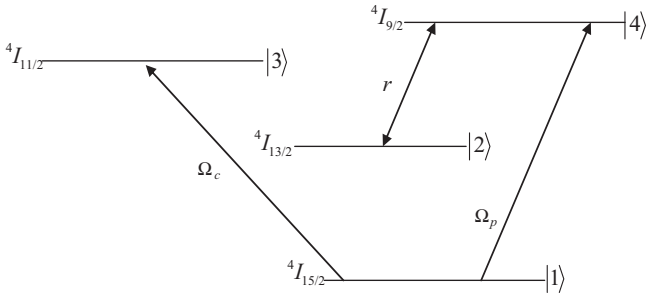

Fig. 2. The Er^{3+}:YAG crystal interacts with two laser fields and an incoherent field. Probe field couples $|1\rangle \leftrightarrow |4\rangle$ transition, and control field drives $|1\rangle \leftrightarrow |3\rangle$ transition. An incoherent pump field with the pumping rate r is acting on $|2\rangle \leftrightarrow |4\rangle$ transition.

phenomenological addition of incoherent pumping and relaxation processes, the elements of density matrix equations can be calculated. If we take the level $|1\rangle$as the energy origin and choose$H_0 = (\omega_p + \omega_c)|4\rangle\langle 4| + \omega_p|2\rangle\langle 2|$, in the interaction picture and under the rotating-wave approximation, the interaction Hamiltonian of the system is given as follows:

$$H_I = -(\Delta_c + \Delta_p)|4\rangle\langle 4| - \Delta_p|2\rangle\langle 2| - (\Omega_c|4\rangle\langle 2| + \Omega_p|2\rangle\langle 1| + HC) \quad (1)$$

where the detuning parameters are defined as$\Delta_c = \omega_{42} - \omega_c$, $\Delta_p = \omega_{21} - \omega_p$, where $\omega_{ij}$is the frequency difference of levels $|i\rangle$and$|j\rangle$, and $\omega_p(\omega_c)$ is the frequency of probe (coupling) field. The corresponding Rabi-frequencies of coupling and probe fields are defined as $\Omega_c = \mu_{42}E_c/2\hbar$and $\Omega_p = \mu_{21}E_p/2\hbar$ where μ_{42}denotes the reduced electric dipole moments of $|4\rangle \leftrightarrow |2\rangle$transition, while μ_{21}signifies the electric dipole moments associated with$|2\rangle \leftrightarrow |1\rangle$. Here we assume the Rabi-frequencies are real. In general Rabi frequencies are complex, but their phase can be absorbed into the other quantities such as the transition operators without loss the generality. In addition E_c and E_p are the amplitude of the coupling and probe fields, respectively. Thus, in rotating wave approximation, the density matrix equations of motion for this system can be obtained as follows: [27]

$$\begin{aligned}
\dot{\rho_{11}} &= -i\Omega_p(\rho_{12} - \rho_{21}) + r(\rho_{33} - \rho_{11}) + \gamma_{21}\rho_{22} + \gamma_{31}\rho_{33} + \gamma_{41}\rho_{44},\\
\dot{\rho_{22}} &= -i\Omega_p(\rho_{21} - \rho_{12}) - i\Omega_c(\rho_{24} - \rho_{42}) - \gamma_{21}\rho_{22} + \gamma_{32}\rho_{33} + \gamma_{42}\rho_{44},\\
\dot{\rho_{33}} &= r(\rho_{11} - \rho_{33}) - \gamma_{31}\rho_{33} - \gamma_{32}\rho_{33} + \gamma_{43}\rho_{44},\\
\dot{\rho_{21}} &= -i\Omega_p(\rho_{22} - \rho_{11}) + i\Omega_c\rho_{41} - (\Gamma_{21} - i\Delta_p)\rho_{21},\\
\dot{\rho_{31}} &= -i\Omega_p\rho_{32} - \Gamma_{31}\rho_{31},\\
\dot{\rho_{41}} &= -i\Omega_p\rho_{42} + i\Omega_c\rho_{21} - (\Gamma_{41} - i\Delta_p - i\Delta_c)\rho_{41},\\
\dot{\rho_{32}} &= -i\Omega_p\rho_{31} - i\Omega_c\rho_{34} - (\Gamma_{32} + i\Delta_p)\rho_{32},\\
\dot{\rho_{42}} &= -i\Omega_c(\rho_{44} - \rho_{22}) - i\Omega_p\rho_{41} - (\Gamma_{42} - i\Delta_c)\rho_{42},\\
\dot{\rho_{43}} &= i\Omega_c\rho_{23} - (\Gamma_{43} - i\Delta_p - i\Delta_c)\rho_{43},
\end{aligned} \quad (2a)$$

where

$$\Gamma_{21}=(\gamma_{21}+r+\gamma_{21}^{dph})/2,$$
$$\Gamma_{31}=(\gamma_{31}+\gamma_{32}+2r+\gamma_{32}^{dph})/2,$$
$$\Gamma_{41}=(\gamma_{41}+\gamma_{42}+\gamma_{43}+r+\gamma_{41}^{dph})/2,$$
$$\Gamma_{32}=(\gamma_{31}+\gamma_{32}+\gamma_{21}+r+\gamma_{32}^{dph})/2,$$
$$\Gamma_{42}=(\gamma_{41}+\gamma_{42}+\gamma_{43}+\gamma_{21}+\gamma_{42}^{dph})/2,$$
$$\Gamma_{43}=(\gamma_{41}+\gamma_{42}+\gamma_{43}+\gamma_{31}+\gamma_{32}+r+\gamma_{43}^{dph})/2. \quad (2b)$$

Here, γ_{ij} are the spontaneous decay rates, and γ_{ij}^{dph} represent the coherence relaxation. The above density matrix elements obey the conditions$\rho_{11}+\rho_{22}+\rho_{33}+\rho_{44}=1$, and $\rho_{ij}=\rho_{ji}^{*}$. The set of Eq. (2a) can be written in the form of one deferential matrix equation:

$$\dot{\mathbf{R}}=-MR+\mathbf{C}, \quad (3)$$

where **R** and **C** are column vectors and M is the matrix of coefficients. The formal solution of such an equation is given by

$$\mathbf{R}(t)=\int_{-\infty}^{t} e^{-M(t-t')}\,\mathbf{C}\,dt'=M^{-1}\,\mathbf{C} \quad (4)$$

We use the above equation to obtain the steady state solution for coherence term.

2.2. Scheme 2

Now, consider a four-level Er^{3+} ionic system in an 35 nm Er^{3+}-doped YAG crystal as shown in Fig. 2. Unlike the previous scheme, in this case, a coherent coupling field with Rabi-frequencyΩ_c, drives the $|3\rangle\leftrightarrow|1\rangle$ transition, decay from level $|3\rangle$ to level $|2\rangle$ populates level$|2\rangle$. An incoherent pump with a pumping rate $r$drives the $|2\rangle\rightarrow|4\rangle$ transition. A weak probe field with Rabi-frequency $\Omega_p$is applied to the $|1\rangle\leftrightarrow|4\rangle$ transition. Similarly with previous section, the density matrix equations of motion in rotating wave approximation can be written as follows:

$$\dot{\rho_{11}}=\gamma_{21}\rho_{22}+\gamma_{31}\rho_{33}+\gamma_{41}\rho_{44}+i\Omega_p(\rho_{14}-\rho_{41})+i\Omega_c(\rho_{13}-\rho_{31}),$$
$$\dot{\rho_{22}}=-\gamma_{21}\rho_{22}+\gamma_{32}\rho_{33}+\gamma_{42}\rho_{44}+r(\rho_{44}-\rho_{22}),$$
$$\dot{\rho_{33}}=-\gamma_{31}\rho_{33}-\gamma_{32}\rho_{33}+\gamma_{43}\rho_{44}-i\Omega_c(\rho_{13}-\rho_{31}),$$
$$\dot{\rho_{41}}=-(\Gamma_{41}+i\Delta_p)\rho_{41}+i\Omega_p(\rho_{44}-\rho_{11})+i\Omega_c\rho_{43},$$
$$\dot{\rho_{31}}=-\Gamma_{31}\rho_{31}+i\Omega_p\rho_{34}+i\Omega_c(\rho_{33}-\rho_{11}),$$
$$\dot{\rho_{43}}=-(\Gamma_{43}+i\Delta_p)\rho_{43}-i\Omega_p\rho_{13}+i\Omega_c\rho_{41},$$
$$\dot{\rho_{21}}=-\Gamma_{21}\rho_{21}+i\Omega_p\rho_{24}+i\Omega_c\rho_{23},$$
$$\dot{\rho_{32}}=-i\Omega_c\rho_{12}-(\Gamma_{32}+i\Delta_c)\rho_{32},$$
$$\dot{\rho_{42}}=-i\Omega_p\rho_{12}-(\Gamma_{42}+i\Delta_p)\rho_{42},$$
$$\rho_{11}+\rho_{22}+\rho_{33}+\rho_{44}=1, \quad (5)$$

where

$$\Gamma_{21}=(\gamma_{21}+r+\gamma_{21}^{dph})/2,$$
$$\Gamma_{31}=(\gamma_{31}+\gamma_{32}+\gamma_{32}^{dph})/2,$$
$$\Gamma_{41}=(\gamma_{41}+\gamma_{42}+\gamma_{43}+r+\gamma_{41}^{dph})/2,$$
$$\Gamma_{32}=(\gamma_{31}+\gamma_{32}+\gamma_{21}+r+\gamma_{32}^{dph})/2,$$
$$\Gamma_{42}=(\gamma_{41}+\gamma_{42}+\gamma_{43}+\gamma_{21}+2r+\gamma_{42}^{dph})/2,$$
$$\Gamma_{43}=(\gamma_{41}+\gamma_{42}+\gamma_{43}+\gamma_{31}+\gamma_{32}+r+\gamma_{43}^{dph})/2. \quad (6)$$

By a similar method the set of Eq. (5) can be solved at steady-state condition. The electric dipole moment between level $i$and level j of Er^{3+} ion, as per [60]is as follows:

$$\mu_{ij}^2=e|\langle\psi|r|\psi'\rangle|^2=\frac{2}{(2J+1)}\frac{2}{(2J'+1)}e^2 \times\sum_{\lambda=2,4,6}\Omega_\lambda\left|\left\langle 4f^N(\alpha SL)J\|U^\lambda\|4f^N(\alpha' S'J')\right\rangle\right|^2 \quad (7)$$

where the eigenvector ψ may be expressed as a linear combination of the unperturbed states corresponding to an arbitrary coupling scheme [61]. $\Omega_\lambda$is the phenomenological intensity parameter, $J$and J' are the quantum numbers of angular momentum of the levels $|i\rangle$, $|j\rangle$, respectively. The factor 2 in Eq. (7) arose from the Kramers degeneration of the Stark levels of Er^{3+} ion. The squared reduced matrix elements $\left|\left\langle 4f^N(\alpha SL)J\|U^\lambda\|4f^N(\alpha' S'J')\right\rangle\right|^2$ can be obtained as per [62] and the spectral intensity parameters can be described by an empirical formula [63]as

$$\Omega_\lambda(10^{-20})=1.25X^{1/4}\exp[-0.4(X-A)^{2/3}]+B \quad (8)$$

where X is the concentration of doped ions and A and B are empirical parameters: $A=1.0, B=0.33$forΩ_2; $A=1.1, B=0.72$ forΩ_4 and $A=1.4, B=0.59$ forΩ_6. From Eqs. (5)–(8), it can be seen that the concentration of doped ions greatly affects Ω_λ; moreover it produces a dramatic influence on μ_{ij}[59]. Based on the experimental results [63], the spectral intensity parameters for the five Er^{3+}:YAG crystals containing Er^{3+} ion concentration of 29.06, 20.57, 17.38, 0.79 and 0.52 at% have been calculated and are listed in Table 1.

Also the population spontaneous emission probability Γ_{ij} of the Er^{3+}:YAG crystals and electrical dipole moments under different concentration are listed in Table 2; [63].

Here, we can estimate the dephasing decay rate as $\gamma_{ij}^{dph}=15\,\Gamma_{21}$ according to [64,65].

Table 1
Spectral intensity parameters of Er:YAG crystals containing different concentrations of the Er^{3+} ion at room temperature [63].

Concentration of Er^{3+} ion crystal (at%)	Spectral intensity parameters (10^{-20} cm^2)		
	Ω_2	Ω_4	Ω_6
0.52	1.16	1.52	1.33
0.79	1.35	1.70	1.47
17.38	0.52	0.92	0.79
20.57	0.47	0.87	0.74
29.06	0.40	0.79	0.66

Table 2
Radiative transitions probabilities and electric dipole momentum of Er^{3+}:YAG crystals containing different concentrations of Er^{3+} ion [63].

Concentration of Er^{3+} ion crystal (at %)	Transition probabilities (s^{-1})						Electric dipole moments (10^{-32} C m	Electric dipole moments (10^{-32} C m)
	Γ_{21}	Γ_{32}	Γ_{31}	Γ_{43}	Γ_{42}	Γ_{41}	μ_{14}	μ_{12}
0.52	239.1	38.4	190.6	10.3	68.3	206.5	2.490	2.102
0.79	258.8	41.1	216.4	16.3	76.6	211	2.618	2.212
17.38	184.6	29.8	128.7	7.6	46.7	127.4	1.920	1.622
20.57	187.8	31.2	129.4	7.9	48	152.4	1.858	1.570
29.06	175.4	29.3	122.3	7.6	44.6	85	1.755	1.463

Now, we consider a medium of length L composed of the above described QW structure immersed in unidirectional ring cavity based on Refs. [35–46,55]. Under slowly varying envelop approximation; the dynamic response of the probe field is governed by Maxwell's equations as follows:

$$\frac{\partial E_p}{\partial t}+c\frac{\partial E_p}{\partial z}=\frac{i\omega_p}{2\varepsilon_0}P(\omega_p). \tag{9}$$

$P(\omega_p)$ is induced polarization in the transitions $|1\rangle\rightarrow|2\rangle$ and $|1\rangle\rightarrow|4\rangle$ for tow models and is given by

$$P(\omega_{p(s)})=N\mu(\rho_{21(41)}) \tag{10}$$

Substituting Eq. (10) into Eq. (9), one can obtain the field amplitude relation for the steady state as follows:

$$\frac{\partial E_p}{\partial z}=i\frac{N\omega_p\mu_{21(41)}}{2c\varepsilon_0}(\rho_{21(41)}) \tag{11}$$

For a perfectly tuned cavity, the boundary conditions in the steady-state limit between the incident field E_p^I and transmitted field E_p^T are as follows:

$$E_p(L)=\frac{E_p^T}{\sqrt{T}} \tag{12}$$

$$E_p(0)=\sqrt{T}E_P^I+RE_p(L), \tag{13}$$

where L is the length of the sample, R is the feedback mechanism and it is responsible for the bistable behavior. Therefore, one does not expect any bistability for $R=0$ in Eq. (13). According to the mean-field limit and by using the boundary conditions the steady state behavior of transmitted field is given by

$$y=2x-i\,C_{21(41)}\,(\rho_{21(41)}) \tag{14}$$

where $y=\mu E_{p(s)}^I/\hbar\sqrt{T}$ and $x=\mu E_{p(s)}^T/\hbar\sqrt{T}$ are the normalized input and output field, respectively. The parameter $C_{21(41)}=N\omega_{p(s)}L|\mu_{21(41)}|^2/2\hbar\varepsilon_0cT$ is the cooperative parameter in a ring cavity. Transmitted field depends on the incident probe field and the coherence terms ρ_{21} and ρ_{41} as given in Eq. (12). In fact, response of the medium to the applied field is determined by the susceptibility χ, which is defined as follows:

$$\chi=\frac{2N\mu_{1j}}{\varepsilon_0E_p}\rho_{j1}\ (j=4,2) \tag{15}$$

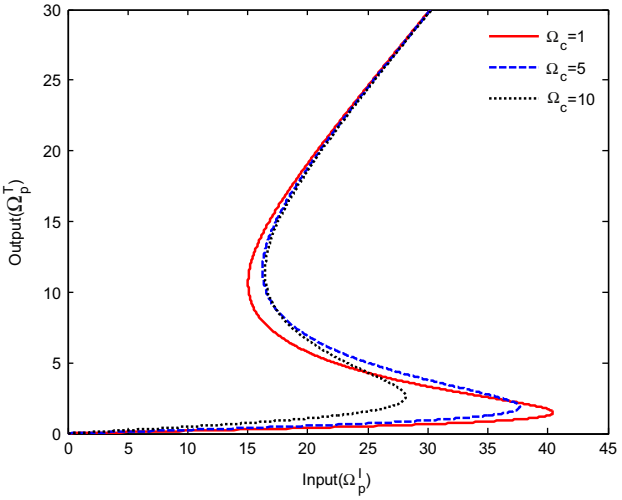

Fig. 3. Plots of the input–output field curves for different values of Rabi frequency Ω_c in the absence of incoherent pumping field for 0.52% Er^{3+} ion concentration. The selected parameters are $\Delta_p=\Delta_c=0$, $r=0$.

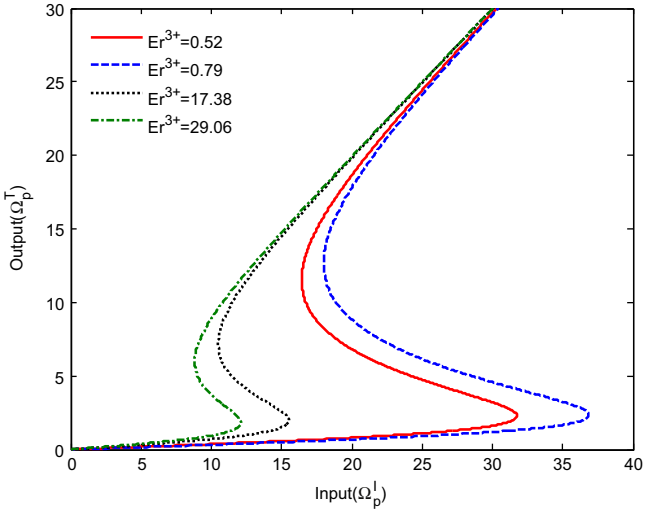

Fig. 5. Plots of the input–output field curves for different values of Er^{3+} ion concentration in the absence of incoherent pumping. The selected parameters are $\Delta_p=\Delta_c=0$, $r=0$.

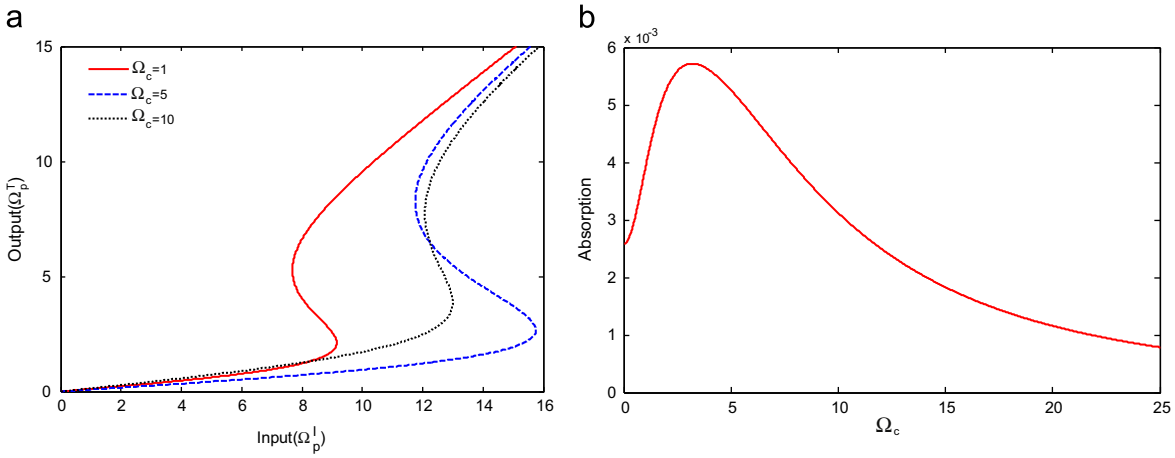

Fig. 4. Plots of the (a) input–output field curves for different values of Rabi frequency Ω_c in the presence of incoherent pumping field and (b) probe absorption versus Rabi frequency Ω_c for 0.52% Er^{3+} ion concentration. The selected parameters are $\Delta_p=\Delta_c=0$, $r=2$.

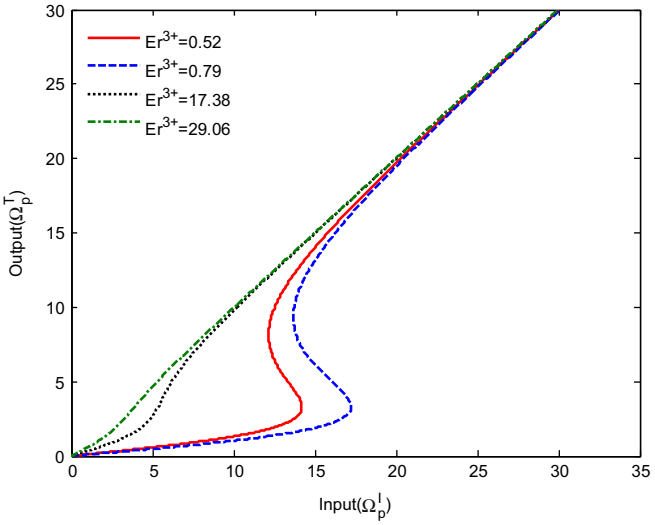

Fig. 6. Plots of the input–output field curves for different values of Er^{3+} ion concentration in the presence of incoherent pumping. The selected parameters are $\Delta_p = \Delta_c = 0,\ r = 2$.

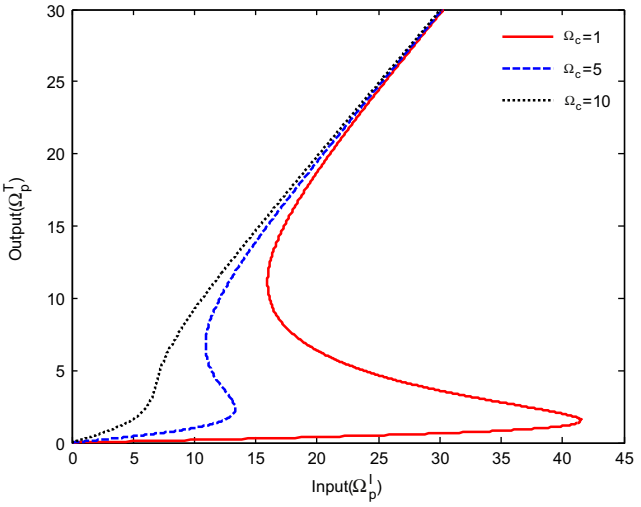

Fig. 7. Plots of the input–output field curves for different values of Rabi frequency Ω_c in the absence of incoherent pumping field for 0.52% Er^{3+} ion concentration. The selected parameters are $\Delta_p = \Delta_c = 0,\ r = 0$.

3. Results and discussion

3.1. Results for scheme 1

The numerical results for the steady state of the output field intensity are given versus the input field intensity with different corresponding parameters as shown in Figs. 3–6. The dependence of the optical bistability on the laser coupling field in the absence of incoherent pumping field and 0.52% Er^{3+} concentration is displayed in Fig. 3. It is found that by increasing the Rabi frequency of coupling field, the bistability threshold decreases. When other parameters are fixed and probe and coupling laser are in resonance with the corresponding transitions ($\Delta_p = \Delta_c = 0$), we can see that OB threshold decreases progressively. Physically, in the absence of incoherent field, the medium is familiar as an EIT ladder type system. In this case, the absorption of the probe field can be reduced by enhancing the coherent field which makes the cavity field easier to reach saturation. The effect of coupling laser field in the presence of incoherent pumping field is shown in Fig. 4. It can be seen that the bistable threshold is dramatically increased as the intensity of the Rabi frequency of coupling field increases, and then decreases gradually. In order to gain a deeper insight into the above result, the absorption coefficients of the probe field versus the Rabi frequency of coupling field is plotted in Fig. 4(b). When the coupling field is absent, the absorption of the medium is suppressed maximally. By increasing the intensity of coupling field, the quantum interference among paths is reduced, which increases the absorption of probe field and makes it harder for the intracavity field to reach saturation. When the coupling field increases to a certain value, the absorption of the probe field reaches a saturation value; the bistable threshold reaches to the maximum. When coupling field further increases, the bistable threshold decreases. Thus, the threshold of OB first increase dramatically with the increase of Rabi frequency and then decreases gradually. The influence of Er^{3+} concentrations on behavior of OB in the absence of incoherent pumping field is displayed in Fig. 5. It is clearly shown that by increasing the Er^{3+} concentration from 0.52% to 0.79%, the threshold of OB enhances. While when the concentration of Er^{3+} continues to increase greatly, the intensity threshold of OB decreases and the area of the hysteresis loop becomes narrower. This indicates that the absorption coefficient for the probe field reaches the maximum at Er^{3+} concentration of about 0.79%, and reaches the minimum at Er^{3+} concentration of about 29.06%. In the following, the dependence of OB on the Er^{3+} concentrations in the presence of incoherent pumping field is analyzed. In Fig. 6, we see numerical results for the steady state of the output field as a function of the input field for different values of Er^{3+} concentration. It is clearly shown that the curves of the cavity input–output field alter with the Er^{3+} concentration. In this case, the results are similar with previous results as shown in Fig. 5. However, the values of OB threshold are less than others. It can be seen that the increasing of the Er^{3+} concentration leads to a significant decrease of the bistable threshold, and the OB disappears when Er^{3+} concentration is 29.06%. It is known that states $|1\rangle$, $|2\rangle$ and $|3\rangle$ are comprised of a standard V-type three-level EIT system, by applying an incoherent pumping field between states $|1\rangle$and $|3\rangle$, we can modify the absorption for the weak probe field on transition $|2\rangle$ to $|1\rangle$.

3.2. Results for scheme 2

The dependence of the optical bistability on the laser coupling field in the absence of incoherent pumping field and 0.52% Er^{3+} concentration based scheme 2 is displayed in Fig. 7. Similar in Fig. 3, it can be seen that by enhancing the Rabi frequency of coupling field the intensity threshold of optical bistability is reduced. However, in this case the values of OB threshold are less than those shown in Fig. 3. Physically, in the absence of incoherent field, the medium is familiar as an EIT V-type system. In this case, the absorption of the probe field can be reduced by enhancing the coherent field which makes the cavity field easier to reach saturation. The effect of coupling laser field in the presence of incoherent pumping field is shown in Fig. 8. It is found that firstly by enhancing the Rabi frequency of coupling filed from 1 to 5 the intensity threshold of optical bistability decreases and the OB disappears. While when Rabi frequency of coupling field changes 5 to 10, the threshold of OB increases. However, in this case the threshold of OB is less than $\Omega_c = 1$. Physically, the absorption coefficients of the probe field versus the Rabi frequency of coupling field are plotted in Fig. 8(b). It can be seen that for $\Omega_c = 1$, there is a probe amplification in the medium and by enhancing the Rabi frequency Ω_c to 5, the EIT occurs easily and the absorption of the probe field is equal to zero. Consequently the OB disappears accordingly. On increasing Ω_c further from 5 to 10, the absorption of the probe field is enhanced, thus the threshold value of the OB

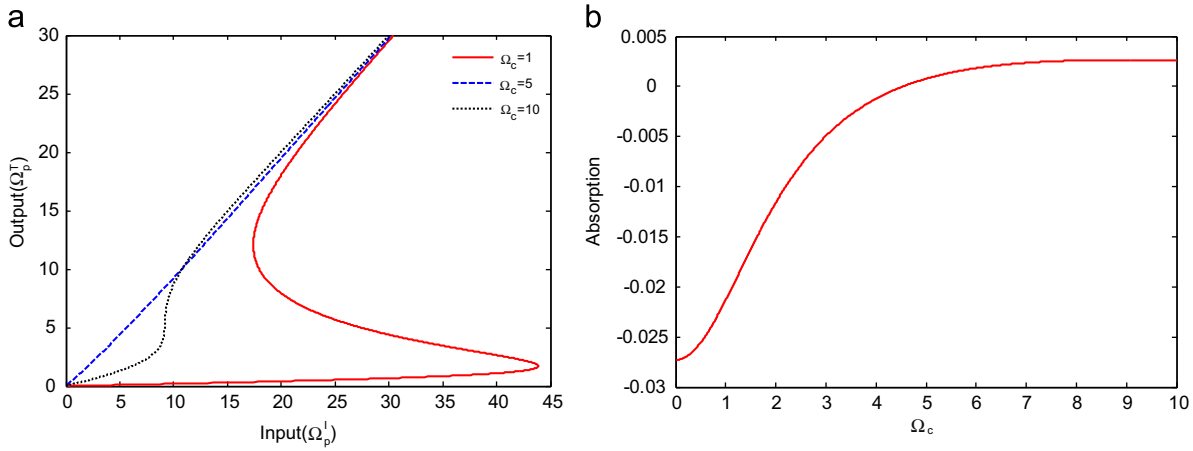

Fig. 8. Plots of the (*a*) input–output field curves for different values of Rabi frequency Ω_c in the presence of incoherent pumping field and (b) probe absorption versus Rabi frequency Ω_c for 0.52% Er^{3+} ion concentration. The selected parameters are$\Delta_p = \Delta_c = 0,\ r = 2$.

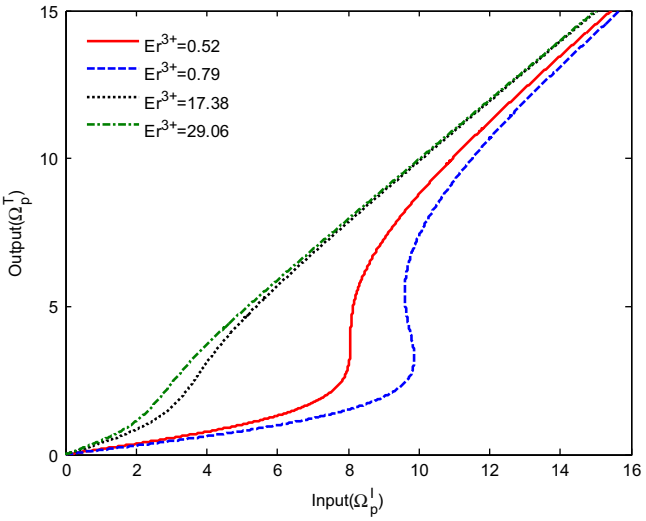

Fig. 9. Plots of the input–output field curves for different values of Er^{3+} ion concentration in the absence of incoherent pumping. The selected parameters are$\Delta_p = \Delta_c = 0,\ r = 0$.

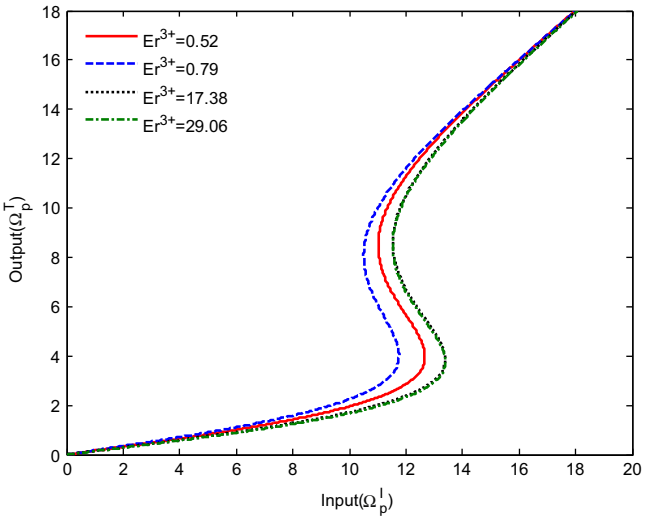

Fig. 10. Plots of the input–output field curves for different values of Er^{3+} ion concentration in the presence of incoherent pumping. The selected parameters are$\Delta_p = \Delta_c = 0,\ r = 2$.

increases considerably and the area of the hysteresis cycle becomes broader. The impact of Er^{3+} concentrations on behavior of OB in the absence of incoherent pumping field is displayed in Fig. 9. It is clearly shown that by increasing the Er^{3+} concentration from 0.52% to 0.79%, the threshold of OB enhances. While when the concentration of Er^{3+} continues to increase greatly, the intensity threshold of OB decreases and the area of the hysteresis loop become narrower. Similar, as shown in Fig. 5, OB threshold reaches the maximum and minimum at Er^{3+} concentration of about 0.79% and 29.06% respectively. However, the threshold value of OB is less than that shown in Fig. 5. Finally, the effect of Er^{3+} concentration on the cavity input–output field in the presence of incoherent pumping field is shown in Fig. 10. It is clearly shown that the curves of the cavity input–output field alter with the Er^{3+} concentration. It is found that by increasing the Er^{3+} concentration from 0.52% to 0.79%, the threshold of OB reduces. While when the concentration of Er^{3+} continues to increase greatly, the intensity threshold of OB increases and the area of the hysteresis loop becomes wider. In this case, maximum and minimum values for OB threshold occur at 29.06% and 0.79% Er^{3+} concentration. These results are completely different with previous results as shown in Figs. 5, 6 and 9. Therefore, it can be found that incoherent pumping field has an essential role to controlling the OB threshold at different Er^{3+} ion concentrations. In this case, by consideration of incoherent pumping field, it gets harder for the probe field to reach saturation which increases threshold of OB . Physically, incoherent pumping field in scheme 2 has an essential role to in producing gain in the medium. Here, quantum coherence between levels $|2\rangle$and $|4\rangle$ will be destroyed by incoherent pumping from level $|2\rangle$to level$|4\rangle$. Consequently, population in upper levels cannot be trapped leading to enhancement of probe gain. So enhancement of probe gain in the medium makes it harder for the field to reach saturation.

4. Conclusion

In summary, we have proposed two atomic models for realizing OB in Er^{3+}:YAG crystal by incoherent pumping field and a laser coupling field. We discuss the effects of Rabi-frequency of applied field, and Er^{3+} ion concentration in the presence and absence of incoherent pumping field on the behavior of OB. Our numerical results show that the threshold power of OB can be reduced or enhanced at different values of Er^{3+} ion concentration. Comparing the results of the two models, we found that Er^{3+} ion concentration

has different effects in the absence or presence of incoherent pumping field. In the present paper, we have reported a preliminary study for optimizing and controlling the optical bistability in Er^{3+}: YAG crystal and provide a basis for choosing the concentration to carry out experimental studies in future.

References

[1] S.E. Harris, Phys. Today 50 (1999) 36.
[2] Y. Wu, X. Yang, Phys. Rev A 71 (2005) 053806.
[3] Y. Zhao, D. Huang, C. Wu, J. Opt. Soc. Am. B 13 (1996) 1614.
[4] M. Sahrai, H. Tajalli, K.T. Kapale, M.S. Zubairry, Phys. Rev. A 70 (2004) 023813.
[5] Y. Wu, Phys. Rev. A 71 (2005) 053820.
[6] Y. Wu, X. Yang, Phys. Rev. A 70 (2004) 053818.
[7] Y. Wu, J. Saldana, Y. Zhu, Phys. Rev. A 67 (2003) 013811.
[8] J.H. Li, X. Yang, Eur. Phys. J. B 53 (2006) 449.
[9] Y. Wu, Y. Deng L, Opt. Lett. 29 (2004) 2064.
[10] J.H. Li, X.Y. Lü, J.M. Luo, Q.J. Huang, Phys. Rev. A 74 (2006) 035801.
[11] A. Joshi, M. Xiao, J. Mod. Opt. 57 (2010) 1196.
[12] S.H. Rahimpour Asadpour, H. Soleimani, Opt. Commun. 315 (2014) 347.
[13] K.I. Osman, Opt. Commun. 259 (2006) 194.
[14] K.I. Osman, A. Joshi, Opt. Commun. 293 (2013) 86.
[15] S.H. Asadpour, A. Eslami-Majd, J. Lumin. 132 (2012) 1477.
[16] Y. Wu, X. Yang, Phys. Rev. Lett. 98 (2007) 013601.
[17] Y. Wu, X. Yang, Phys. Rev. A. 76 (2007) 013832.
[18] Z. Wang, T. Shui, B. Yu, Opt. Commun. 315 (2014) 263.
[19] S.H. Asadpour, M. Sahrai, A. Soltani, H.R. Hamedi, Phys. Lett A. 376 (2012) 147.
[20] M. Sahrai, S.H. Asadpour, R. Sadighi- Bonabi, J. Non-Opt. Phys. 19 (2010) 503.
[21] T. Naseri, S.H. Asadpour, R. Sadighi-Bonabi, J. Opt. Soc. Am. B 30 (2013) 641.
[22] Z. Wang, B. Yu, Laser Phys. Lett. 11 (2014) 035201.
[23] J.H. Li, R. Yu, X. Yang, Appl. Phys. B 111 (2013) 65.
[24] A. Joshi, S.H. Shoukry, M. Xiao, Phys. Rev. A 72 (2005) 055803.
[25] D. Zhang, J.H. Li, C. Ding, X. Yang, Phys. Lett. A 376 (2012) 1978.
[26] B.S. Hum, P.R. Hemmer, M.S. Shahriar, Opt. Commun. 144 (1997) 227.
[27] H.F. Zhang, J.H. Wu, X.M. Su, J.Y. Gao, Phys. Rev. A. 66 (2002) 053816.
[28] Y. Zhao, C.K. Wu, B.S. Ham, M.K. Kim, E. Awad, Phys. Rev. Lett. 79 (1997) 641.
[29] K. Ichimura, Y. Yamamoto, N. Gemma, Phys. Rev. A 58 (1998) 4116.
[30] D.E. Nikonov, A. Imamoglu, M.O. Scully, Phys. Rev. B 59 (1999) 12212.
[31] A. Imamoglu, R.J. Ram, Opt. Lett. 131 (1996) 333.
[32] C.R. Lee, Appl. Phys. Lett. 86 (2004) 201112.
[33] M.D. Frogley, J.F. Dynes, M. Beck, J. Faist, C.C. Philips, Nat. Mater. 5 (2006) 175.
[34] R. Atanasov, A. Hache, J.L.P. Hughes, H.M. Van Driel, J.E. Sipe, Phys. Rev. Lett. 76 (1996) 1703.
[35] J.H. Li, *Phys Rev B.* 75 (2007) 155329.
[36] J.H. Li, Opt. Commun. 274 (366) (2007) 2007.
[37] A. Joshi, M. Xiao, Appl. Phys. B: Lasers Opt. 79 (2004) 65.
[38] Z. Wang, H. Fan, J. Lumin. 130 (2010) 2084.
[39] Z. Wang, S. Zhen, X. Wu, J. Zhu, Z. Cao, B. Yu, Opt. Commun. 304 (2013) 7.
[40] Z. Wang, B. Yu, J. Opt. Soc. Am. B 30 (2013) 2915.
[41] D. Zhang, R. Yu, J.H. Li, C. Ding, X. Yang, Phys. Lett. A 377 (2013) 2621.
[42] J.H. Li, X. Hao, J. Liu, X. Yang, Phys. Lett. A 372 (2008) 716.
[43] Z. Wang, B. Yu, J. Appl. Phys. 113 (2013) 113101.
[44] Z. Wang, Opt. Commun. 282 (2009) 4745.
[45] Z. Wang, B. Yu, S. Zhen, X. Wu, J. Zhu, Z. Cao, Superlattices Microstruct. 51 (2012) 324.
[46] S.H. Asadpour, M. Jaberi, H. Rahimpour Soleimani, J. Opt. Soc. B 30 (2013) 1815.
[47] W.W. Chow, H.C. Schneider, M.C. Phillips, Phys. Rev. A 68 (2003) 053802.
[48] J. Kim, O. Benson, H. Kan, Y. Yamamoto, Nature (London) 397 (1999) 500.
[49] P. Michler, Science 290 (2000) 2282.
[50] Y. Yamamoto, Phys. Rev. Lett. 89 (2002) 233602.
[51] H. Xu, Z. Dai, Z. Jiang, Phys. Lett. A 294 (2002) 19.
[52] H. Ghaforyan, H.R. Hamedi, A. Khaledi-Nasab, H. Jafarzadeh, S.H. Asadpour, S.M. Hosseini, M. Sahrai, J. Mod. Opt. 60 (2013) 674.
[53] M. Sahrai, S.H. Asadpour, A. Eslami-Majd, R. Sadighi- Bonabi, J Mod. Opt. 59 (2012) 446.
[54] Z. Wang, Opt. Commun. 283 (2010) 3291.
[55] Z. Wang, J. Lumin. 131 (2011) 2404.
[56] Z. Zang, Appl. Opt. 52 (2013) 5701.
[57] Z. Zang, W.X. Yang, J. Appl. Phys. 109 (2011) 103106.
[58] Z. Zang, Y. Zhang, J. Mod. Opt. 59 (2012) 161.
[59] Z. Zang, Y. Zhang, Appl. Opt. 51 (2012) 3424.
[60] B.R. Judd, Phys. Rev. 127 (1962) 750;
G.S. Ofelt, J. Chem. Phys. 37 (1962) 511.
[61] G.S. Ofelt, J. Chem. Phys. 37 (1962) 511.
[62] A.A. Kaminski, V.S. Mironov, A. Kornienko, S.N. Bagaev, G. Boulon, A. Brenier, B. Di Bartolo, Phys. Status Solidi A 151 (1995) 231.
[63] Q.Y. Wang, S.Y. Zhang, Y.Q. Jia, J. Alloys Compd. 202 (1993) 1.
[64] H.F. Zhang, Z.W. Dai, B. Zhang, Wu J.H. Gao, J. Y, Chin. Phys. 12 (2003) 964.
[65] Y. Sun, C.W. Thiel, R.L. Cone, R.W. Equall, R.L. Hutcheson, J. Lumin. 98 (2002) 281.